Exp Fluids (2013) 54:1511
DOI 10.1007/s00348-013-1511-9

RESEARCH ARTICLE

An experimental study of flow fields and wind loads on gable-roof building models in microburst-like wind

Yan Zhang · Partha Sarkar · Hui Hu

Received: 17 September 2012 / Revised: 25 March 2013 / Accepted: 27 March 2013 / Published online: 8 May 2013

Abstract An experimental study was conducted to quantify the flow characteristics of microburst-like wind and to assess the resultant wind loads acting on low-rise, gable-roof buildings induced by violent microburst-like winds compared with those in conventional atmospheric boundary layer winds. The experimental work was conducted by using an impinging-jet-based microburst simulator in the Department of Aerospace Engineering, Iowa State University. Two gable-roof building models with the same base plan and mean roof height, but different roof angle, were mounted over a homogenous flat surface for a comparative study. In addition to measuring the surface pressure distributions to determine the resultant wind loads acting on the building models, a digital particle image velocimetry system was used to conduct flow field measurements to reveal the wake vortex and turbulence flow structures around the building models placed in the microburst-like wind. The effects of important parameters, such as the distance of the building from the center of the microburst, the roof angle of the building, and the orientation of the building with respect to radial outflow of the oncoming microburst-like wind, on the flow features such as the vortex structures and the surface pressure distributions around the building models as well as the resultant wind loads acting on the test models were assessed quantitatively. The measurement results reveal clearly that when the building models were mounted within the core region of the microburst-like wind, the surface pressure distributions on the building models were significantly higher than those predicted by ASCE 7-05 standard, thereby induced considerably greater downward aerodynamic forces acting on the building models. When the building models were mounted in the outflow region of the microburst-like wind, the measured pressure distributions around the building models were found to reach a good correlation with ASCE 7-05 standard gradually as the test models were moved far away from the center of the microburst-like wind. It was also found that both the radial and vertical components of the aerodynamic forces acting on the building models would reach their maximum values when the models were mounted approximately one jet diameter away from the center of the microburst-like wind, while the maximum pressure fluctuations on the test models were found to occur at further downstream locations. Roof angles of the building models were found to play an important role in determining the flow features around the building models and resultant wind loads acting on the test models. The flow field measurements were found to correlate with the measured surface pressure distributions and the resultant wind loads (i.e., aerodynamic forces) acting on the building models well to elucidate the underlying physics of flow-structure interactions between the microburst-like winds and the gable-roof buildings in order to provide more accurate prediction of the damage potentials of the microburst wind.

Y. Zhang · P. Sarkar · H. Hu (✉)
Department of Aerospace Engineering, Iowa State University, Ames, IA 50011-2271, USA
e-mail: huhui@iastate.edu

1 Introduction

A downburst, which is characterized by a strong localized downdraft flow and an outburst of strong wind near the ground surface, occurs within a thunderstorm where the weight of the precipitation and the cooling due to microphysical processes acts to accelerate the airflow downwards. Based on the 2001 Extreme Weather Sourcebook of

National Center for Atmospheric Research (NCAR), approximately 5 % of thunderstorms would produce a downburst that is primarily responsible for the estimated \$1.4B of insured property loss each year in USA alone (data taken from 1950–1997). A microburst, as defined by Fujita (1985), is a strong downburst which produces an intense outburst of damaging wind with the radial extent being less than 4.0 km, or else is defined as a macroburst. Although a “microburst” has a smaller size than its counterpart, “macroburst”, it could induce a much stronger outflow with the maximum wind speed up to 270 km/h, i.e., 170 mph (Fujita 1985).

As shown schematically in Fig. 1, the flow characteristics of a microburst are dramatically different from those of conventional “straight-line” atmospheric boundary layer (ABL) winds (Kaimal and Finnigan 1994) and other wind hazards of wide concerns, e.g., tornadoes and gust fronts. While a microburst is usually conceived as an upside-down tornado due to its basic flow pattern, in contrast to tornado-like winds (Bluestein and Golden 1993; Yang et al. 2011), microbursts produce negligible tangential-velocity components and behave more like purely straight-line winds in the outburst regions far away from the core regions of the microbursts. Unlike conventional ABL winds, a microburst can produce an impinging-jet-like outflow profile diverging from its center with the maximum velocity occurring at an altitude of less than 50 m above ground (Hjelmfelt 1988).

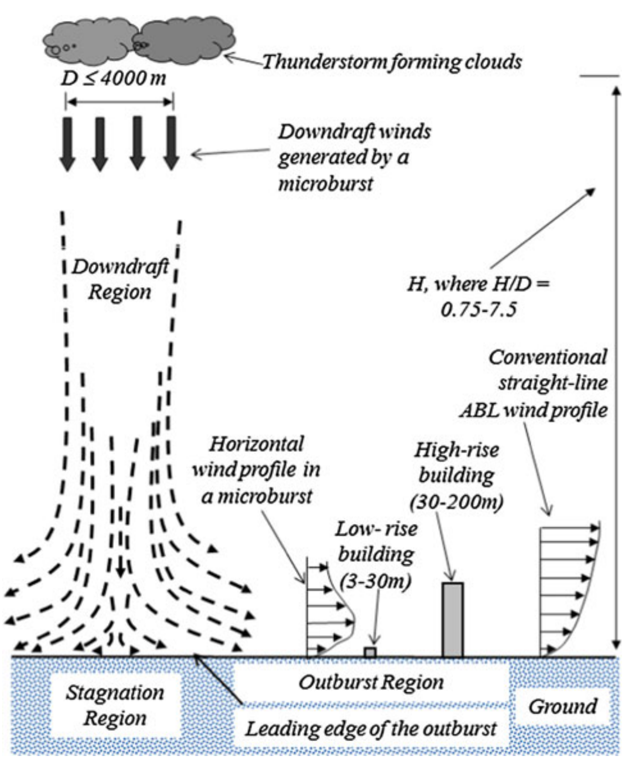

Fig. 1 Schematic of a microburst

Such extreme high wind speed and wind shear (i.e., velocity gradient) near the ground could produce a significantly greater damaging potential to low-rise built structures compared to those of conventional ABL wind. Furthermore, in contrast to conventional ABL wind, microbursts could have strong vertical velocity components in both the core regions and the leading edges of the outburst, as shown in Fig. 1, which can be extremely dangerous with respect to the safety of aircraft as well as to the built structures on the ground. As a result, it is highly desirable to characterize the flow features of the microburst wind in order to elucidate the underlying physics to provide more accurate prediction of the damage potentials of the microburst wind to both aviation industry and the low-rise built structures.

Initiated by a meteorological investigation of the 1976 Eastern 66 aircraft crash at New York City’s JFK airport, several studies have been conducted by meteorologists as well as engineering researchers to quantify the flow characteristics of microburst wind. During 1970s and 1980s, two major research projects, the Northern Illinois Meteorological Research on Downburst (NIMROD, Chicago, IL) and the Joint Airport Weather Studies (JAWS, Denver, CO), were carried out to gather field data to quantify the microbursts occurring in nature. The field research efforts were documented in Fujita (1979), Wilson et al. (1984), Hjelmfelt (1987), and Hjelmfelt (1988). Meanwhile, a number of other field studies were also conducted at various locations. For example, Atlas et al. (2004) investigated the physical origin of a microburst occurring in the Amazonia region of South America by using a set of Doppler Radar data. Vasiloff and Howard (2008) deployed two types of Radar systems to capture data from a severe microburst occurring near Phoenix, Arizona. While the field studies provided valuable measurement data to depict a vivid picture of microburst wind, only limited quantitative information could be obtained through those field studies due to the technical challenges and intrinsic limitations of the Doppler Radar detection systems used in the field measurements (i.e., low scanning frequency and poor spatial resolution near ground). The limitations of field studies make laboratory experiments with microburst simulators and scaled test models essential tools to provide more detailed information about the flow characteristics of the microburst-like wind near the ground and their interactions with built civil structures in order to assess their destructive potentials.

While a typical microburst in nature is found to have a lifetime about 10 min, a steady impinging-jet flow was found to resemble the major features of a microburst at its maximum strength reasonably well (Hjelmfelt 1987). Therefore, steady impinging-jet model has been widely adopted to simulate microburst-like wind in laboratory experiments due to its simplicity and ability to produce outflow velocity profiles resembling that of microburst wind. A number of numerical and experimental studies have been conducted in the past years to utilize the steady impinging-jet model to investigate the flow characteristics of microburst-like wind. Selvam and Holmes (1992) used a two-dimensional k-ε model to simulate an impinging-jet flow to characterize the flow features of microburst-like winds. Holmes (1999) and Letchford and Illidge (1999) performed experimental studies using an air jet impinging onto a wall to investigate the topographic effects of a microburst on the outflow velocity profiles. Wood et al. (2001) studied the characteristics of microbursts over various terrains, both experimentally and numerically, by using an impinging-jet model. Choi (2004) carried out both field and laboratory measurements to study on a series of Singapore thunderstorms. Terrain sensitivity of microburst outflows was studied by comparing the microburst observations at different heights and impinging-jet experiments with different height-to-diameter ratios. The study produced similar trends, which confirms the good capability of impinging-jet model to simulate microburst-like wind. Chay et al. (2005) conducted numerical simulations of impinging-jet flows and obtained good agreements with the wind-tunnel measurement results of microburst-like wind. To physically capture transient features of microbursts, Mason et al. (2005) suggested a pulsed impinging-jet model to simulate transient microburst phenomena. Holmes and Oliver (2000) empirically combined wall-jet velocity and translational velocity and obtained a good representation of a traveling microburst that was well correlated with a microburst occurred at Andrews AFB in 1983. Kim and Hangan (2007) and Das et al. (2010) performed CFD studies to simulate both steady and transient microbursts using the impinging-jet model, producing reasonable radial-velocity profiles and good primary-vortex representation of microburst-like wind. In summary, the impinging-jet model has been proved to be very effective to simulate microburst wind in laboratory experiments.

With the consideration of buildings as surface-mounted obstacles, extensive experimental and numerical studies have been carried out to investigate the flow-structure interactions between building models and turbulent surface winds as well as the resultant wind loads acting on the building models. Besides the studies using prismatic obstacles to represent cube-shaped buildings, several studies have also been conducted to consider more realistic residential building models with various gable roof shapes (Holmes 1999; Kanda and Maruta 1993; Peterka et al. 1998; Uematsu and Isyumov 1999; Stathopoulos et al. 2001; Sousa 2002; Sousa and Pereira 2004; Liu et al. 2009; Hu et al. 2011) to quantify the effects of the gable-roof shapes on the wake flow characteristics as well as the resultant wind loads acting on the building models. While many important findings have been obtained through the previous studies, most of those studies were conducted with the building models placed in conventional ABL wind.

As aforementioned, a microburst can produce an impinging-jet-like outflow profile diverging from its center with the maximum velocity occurring at an altitude of less than 50 meters above the ground. It has also strong vertical velocity components in both the core region and the leading edge of the outburst flow. Such extreme surface winds and high velocity gradients near the ground could produce much greater damaging effects on low-rise buildings compared with conventional ABL wind. Due to the distinct features of the microburst-like wind, the current design standards of low-rise buildings may not be applicable to estimate the wind loads induced by microburst-like wind, the characteristics of the flow-structure interactions between the low-rise buildings and the devastating microburst wind would be very different from those with conventional ABL wind. Surprisingly, although microbursts are well-known natural hazards, only very few studies can be found in literature to specifically address the flow-structure interactions between microburst-like wind and buildings. Nicholls et al. (1993) conducted a Large Eddy Simulation (LES) study to investigate the flow structures around a cube-shaped building model in microburst-like wind. Savory et al. (2001) utilized an impinging-jet model to investigate the failure of a lattice transmission tower in microburst-like wind. Chay and Letchford (2002), Letchford and Chay (2002) investigated the pressure distribution over a cube-shaped building model in steady and translating microburst-like wind by performing laboratory experiments with an impinging-jet model. More recently, Sengupta and Sarkar (2008) conducted an experimental study to quantify the transient loads acting on a cube-shaped building model with an impinging-jet-based microburst simulator. It should be noted that while most of the previous studies on building models in microburst-like wind were conducted by measuring wind loads and/or surface pressure distributions on cube-shaped building models only, no study can be found in literature to provide flow field measurements to quantify the global flow features of microburst-like winds and the flow-structure interactions between the microburst-like winds and low-rise buildings. Furthermore, while gable-roof buildings are the most common low-rise buildings, which are very vulnerable to microburst wind, many important aspects about the flow-structure interactions between microburst wind and gable-roof buildings as well as the resultant wind loads (e.g., aerodynamics forces) acting on gable-roof buildings induced by the microburst-like wind are still unclear.

In the present study, an experimental study was conducted to quantify the flow characteristics of microburst-like wind and to assess the fluid–structure interactions of gable-roof buildings in microburst-like wind using scaled models. The experimental work was conducted by using an impinging-jet-based microburst simulator located in the Aerospace Engineering Department of Iowa State University (ISU). Two low-rise gable-roof building models with the same base plan and mean-roof height but different roof angles were used for the comparative study. In addition to mapping the surface pressure distributions around the building models to determine the resultant wind loads (i.e., aerodynamic forces) acting on the models in the microburst-like wind, a high-resolution Particle Image Velocimetry (PIV) system was used to conduct flow field measurements to reveal the flow features and wake vortex structures around the gable-roof building models in microburst-like wind. The flow field measurements were correlated with the surface pressure and resultant wind loads measurements in order to elucidate the underlying physics. The effects of important parameters, such as the distance of the building from the center of the microburst, the roof angle and orientation angle of the building with respect to the radial outflow of the oncoming microburst-like wind, on the flow field and surface pressure distributions on the building models (thereby, the resultant aerodynamic forces acting on the models) induced by the microburst-like wind were assessed quantitatively. The objective of the present study is to gain further insight into the underlying physics of the flow-structure interactions of low-rise gable-roof buildings and microburst-like wind for a better understanding of the damage potential of microburst-like wind to low-rise buildings.

2 Experimental setup and ISU microburst simulator

2.1 ISU microburst simulator

The experimental study was conducted by using an impinging-jet-based microburst simulator located in the Aerospace Engineering Department of Iowa State University (ISU). As mentioned earlier, impinging-jet model has been widely used to simulate microburst wind due to its simplicity to produce outflow profiles resembling microburst wind. Two methods are mostly used in previous studies to generate impinging jet flows in laboratory experiments to investigate microburst-like winds. One method is to utilize the density difference between the core jets and ambient surrounding flows to form buoyancy-driven downdrafts, which is usually used to elucidate the underlying physics pertinent to the formation mechanism of microbursts (Alahyari and Longmire 1995). The other method is to use fans/blowers to generate forced jet flows impinging onto ground plates at an iso-thermal condition, which was widely used to assess the global flow features of microburst-like winds and the microburst-induced wind loads acting on building models mounted on the ground plates (Sengupta and Sarkar 2008). While the formation mechanism of microbursts is very complicated and worth further investigations, the assessments of the global flow feature of microburst-like wind and microburst-induced wind loads acting on buildings are also very important topics in wind engineering community. Since the main focus of the present study is to quantify the flow characteristics of microburst-like winds and to assess the resultant wind loads acting on low-rise, gable-roof buildings induced by microburst-like winds, instead of elucidating the formation mechanism of microbursts, the experimental investigations were performed by generating a forced impinging jet flow in the laboratory to simulate microburst-like wind at an iso-thermal condition (i.e., the thermal condition of a microburst in nature was not simulated in the present study).

Figure 2 shows the schematic and photo depicting the flow circuit and dimensions of ISU microburst simulator used in the present study. As shown in Fig. 2, a downdraft flow is generated through an axial fan driven by a step motor. The exhaust nozzle diameter of ISU microburst simulator is 610 mm (i.e., $D = 610$ mm). The distance between the nozzle exit and the ground plane (H) is adjustable up to 2.3 times the nozzle diameter. Honeycomb

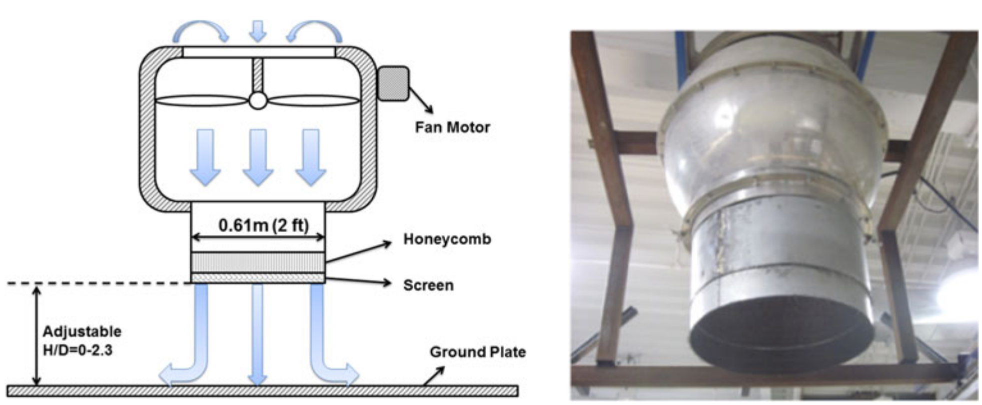

Fig. 2 A schematic and photo of ISU microburst simulator

and screen structures are placed upstream of the nozzle exit in order to produce a uniform jet flow exhausted from ISU microburst simulator. During the experiments, a three-component cobra-probe (Turbulent Flow Instrumentation Pvt. Ltd.®), which is capable of simultaneously measuring all three components of the wind velocity vector, was used to quantify the flow characteristics of the jet flow at the points of interest. It was found that the jet flow exhausted from ISU microburst simulator was quite uniform across the nozzle exit, and the turbulence level of the core jet flow was found to be within 1.0 %. For most of the measurement results given in the present study, the ground floor was fixed at *2D* below the ISU microburst simulator (i.e., $H/D = 2.0$). The flow velocity at the nozzle exit of the ISU microburst simulator was set to 6.0 m/s (i.e., $U_{\text{jet}} = 6.0\,\text{m/s}$), which corresponds to a Reynolds number of 2.4×10^5 based on the nozzle diameter, *D*, of the ISU microburst simulator. Further information about the design, construction, and performance of ISU microburst simulator as well as the quantitative comparisons of the microburst-like wind generated by using the simulator with the microbursts occurring in nature can be found in Zhang et al. (2012).

It should be noted that dynamic similarity is one of the greatest challenges to conduct laboratory experiments to simulate meteorological phenomena such as microbursts. It will be very difficult, if not impossible, to match the Reynolds numbers of the microbursts in nature with those of the impinging jet flows generated in the laboratories due to the significant scale difference of the two cases. It has been found that although the Reynolds numbers of the laboratory experiments may not be able to match to those of microbursts in nature, the measurement results obtained from laboratory experiments are still very useful to reveal the flow characteristics of microburst-like winds and to predict the winds loads acting on test models induced by microburst-like wind as long as the Reynolds number of the laboratory experiments is high enough (i.e., $Re > 10^5$). Therefore, the findings derived from the present study are believed to be very helpful to improve our understanding about the flow characteristics of microburst-like winds and flow-structure interactions between the microburst-like winds and the gable-roof buildings in order to provide more accurate prediction of the damage potentials of the microburst wind.

2.2 The gable-roof building models

Figure 3 shows the schematic of the two gable-roof building models used in the present study: one with a roof angle of 16° and the other with a roof angle of 35°. The two models were designed to have the same square shaped base plan and the same mean roof height. The primary design parameters of the test models (i.e., both the absolute values and non-dimensional values normalize by the diameter of the microburst simulator, *D*) are listed in Table 1. With the scale ratio of the 1:650, the test models used in the present

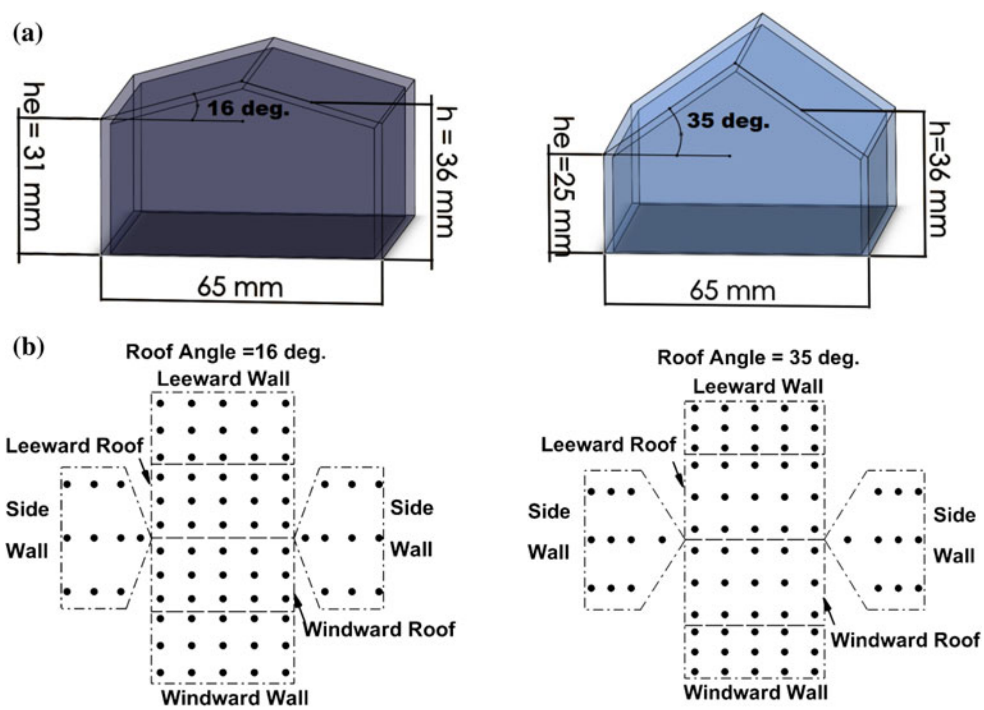

Fig. 3 The schematic of the two gable-roof building models used in the present study. **a** Prospective views of the two gable-roof building models **b** stretched-out view of the building models to show the locations of the pressure taps

Table 1 Primary design parameters of the building models used in present study

Test model	Model #1 with 16° roof angle		Model #2 with 35° roof angle	
	Absolute value (mm)	Non-dimensional value (L/D)	Absolute value (mm)	Non-dimensional value (L/D)
Mean roof height of the test model	36.0	0.059	36.0	0.059
Eave height of the test model	31.0	0.051	25.0	0.041
Total height of the test model	38.5	0.063	41.5	0.068
Base size of the test model	65.0	0.107	65.0	0.107
Mounted location of the model relative to the microburst simulator center	r/D $\approx$ 0, 0.5, 1.0, 1.5, 2.0		r/D $\approx$ 0, 0.5, 1.0, 1.5, 2.0	

study would represent gable-roof buildings with about 42 m $\times$ 42 m in base plan and 23 m in mean-roof-height interacting with a microburst of 400 m in diameter.

As shown in Fig. 3b, each of the test models was equipped with 80 pressure taps for the surface pressure distribution measurements around the model. The pressure taps were connected to two ZOC pressure sensor systems (Scanivalve Corp.®) by using tygon tubing (1.5 mm in diameter and 0.8 m long) for the surface pressure data acquisition. The ZOC pressure sensor systems incorporate temperature-compensated piezoresistive pressure sensors with a pneumatic calibration valve, RAM, 16 bit A/D converter, and a microprocessor in a compact self-contained module. The precision of the pressure acquisition system is ±0.2 % of the full scale (±10 in. H2O). During the experiments, the instantaneous surface pressure measurement data were acquired for 100 s with data acquisition rate of 100 Hz for each test case.

During the experiments, the surface pressure distributions, $C_P = (P - P_{\mathrm{atm}})/(0.5\rho U_{\mathrm{jet}}^2)$, on the test models were measured with the models located at different radial distances from the center of the impinging jet, i.e., at r/D $\approx$ 0.0, 0.5, 1.0, 1.5, and 2.0. As shown in Fig. 4, the test models were also mounted at three different orientation angles, i.e., 0°, 45°, and 90°, with respect to the oncoming microburst-like wind at each downstream location. The resultant wind loads (i.e., aerodynamic forces) acting on the test models were determined by integrating the surface pressure distributions around the test models.

In addition to the surface pressure distribution and resultant wind load measurements, a high-resolution Particle Image Velocimetry (PIV) system was used to quantify the flow characteristics of the microburst-like wind around the gable-roof building models. For the PIV measurements, the airflow was seeded with $\sim$1 μm oil droplets by using a droplet generator. As shown in Fig. 4, illumination was provided by a double-pulsed Nd/YAG laser (NewWave Gemini 200) adjusted at the second harmonic frequency and emitting two 200 mJ laser pulses at a wavelength of 532 nm and a repetition rate of 10 Hz. The laser beam was shaped into a laser sheet (thickness $\sim$1 mm) by using a set of spherical and cylindrical lenses. A high-resolution charge-coupled device (CCD) camera (PCO1600, Cooke Corp.) was used for PIV image acquisition with its view axis perpendicular to the illuminating laser sheet. The CCD camera and the double-pulsed Nd/YAG lasers were connected to a workstation via a Digital Delay Generator (Berkeley Nucleonics, Model 565), which controlled the timing of both the laser illumination and the image acquisition. Instantaneous PIV velocity vectors were obtained using a frame-to-frame cross-correlation technique involving successive frames of image patterns of particle images in an interrogation window of 32 $\times$ 32 pixels. An effective overlap of 50 % of the interrogation windows was employed in PIV image processing. After the instantaneous velocity vectors were derived, time-averaged quantities, such as the mean velocity (V_r, V_z), turbulent velocity fluctuations (v'_r, v'_z) and the normalized turbulent kinetic energy (i.e., $T.K.E. = (\overline{v'_r v'_r} + \overline{v'_z v'_z})/U_{\mathrm{jet}}^2$) of the turbulent flow, were obtained from a time sequence of 1,000 frames of the instantaneous PIV measurement results for each test case. The uncertainty level for the instantaneous PIV measurements is estimated to be within 2.0 %, and those of the turbulent velocity fluctuations and turbulent kinetics energy are about 5.0 %.

In the present study, the size of each PIV measurement window was set to be about 210 mm $\times$ 160 mm in order to ensure a reasonable good spatial resolution of the PIV measurements (i.e., $\sim$2.0 mm). Since this measurement window is quite small compared with the dimension of ISU microburst simulator ($D = 0.61$ m), the PIV measurement results from 14 different measurement windows were combined to reveal the global features of the microburst-like wind generated by ISU microburst simulator more clearly. The layout of the 14 PIV measurement windows is illustrated in Fig. 4b.

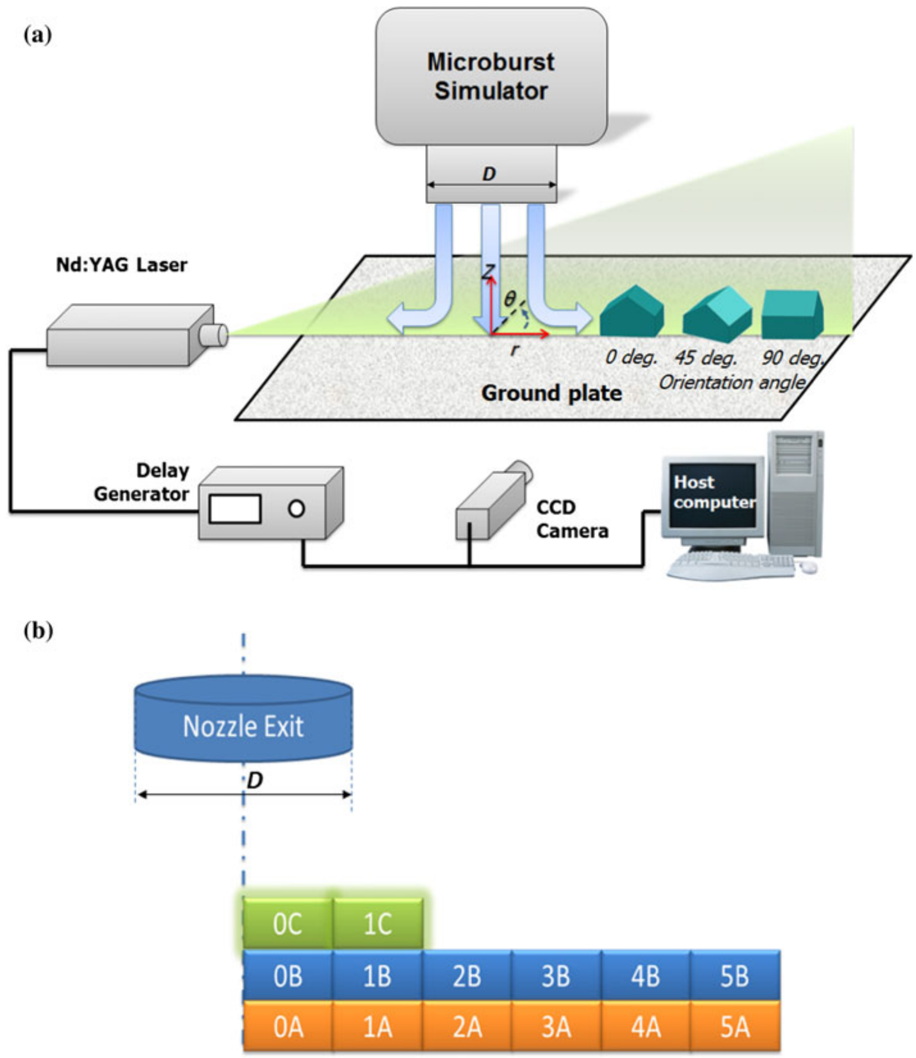

Fig. 4 Schematic of the experimental setup used in the present study **a** the experimental setup for PIV measurements **b** layout of the PIV measurement windows

3 Results and discussions

3.1 The flow characteristics of the simulated microburst-like wind

In the present study, the flow characteristics of the microburst-like wind generated by ISU microburst simulator were quantified by using the high-resolution PIV system before the gable-roof building models were mounted on the ground plane. As described above, PIV measurement results from 14 different measurement windows were combined to reconstruct a large flow field (~0.4 m × 1.5 m) in order to reveal the flow features of the microburst-like wind more clearly. Figure 5 shows the reconstructed flow field in the terms of the flow velocity vectors (only about 1.5 % of the vectors are shown here), the contour maps of the radial and vertical velocity components (V_r, V_z), and the normalized turbulent kinetic energy (i.e., normalized T.K.E) as well as the streamlines of the microburst-like wind in the measurement windows. It can be seen clearly that the streamlines of the jet flow exhausted from ISU microburst simulator are mainly vertical in downward direction before impinging onto the ground plane, as expected. As a result, the microburst-like wind was found to have a strong vertical component in the core region and the leading edge of the outburst region (i.e., r/D ≤ 0.5), which are dangerous to the safety of aircraft as well as built structures on the ground. Upon impinging onto the ground plane, the flow was found to turn right angle rapidly, and the corresponding streamlines were found to become horizontal lines in the outburst flow. While diverging away from the core center of the microburst-like wind, the flow was found to be accelerated at first, reach its maximum wind speed at the location of r/D ≈ 1.0, and then slow down gradually at further downstream. Since the radial velocity component (i.e., V_r component) was found to become dominant in the outflow region of the microburst-like wind (i.e., r/D > 0.50), the

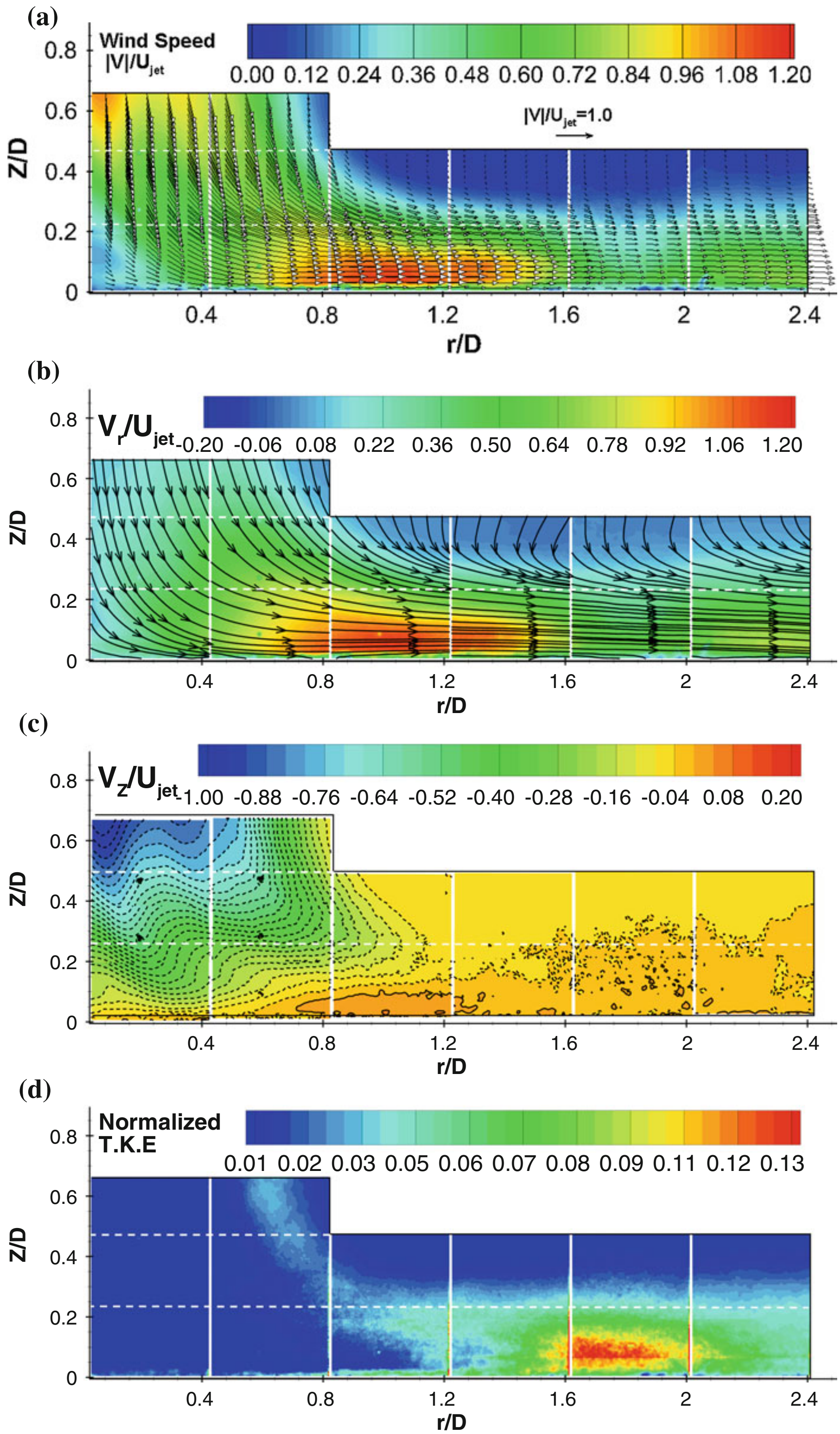

Fig. 5 PIV measurement results of the microburst-like wind **a** time-averaged flow velocity vectors **b** distribution of radial velocity, V_r **c** distribution of vertical velocity, V_Z **d** distribution of turbulence kinetic energy (T.K.E)

streamlines of the flow in the outburst flow were found to become parallel straight lines near the ground plane. It indicates that the microburst-like wind would behave more like a straight-line wind in the outflow region near the ground plane.

It should be noted that even though the streamlines of the microburst-like wind in the outflow region were found to become parallel straight-lines, the flow characteristics of the microburst-like wind were still quite different from those in conventional ABL winds. As revealed clearly from

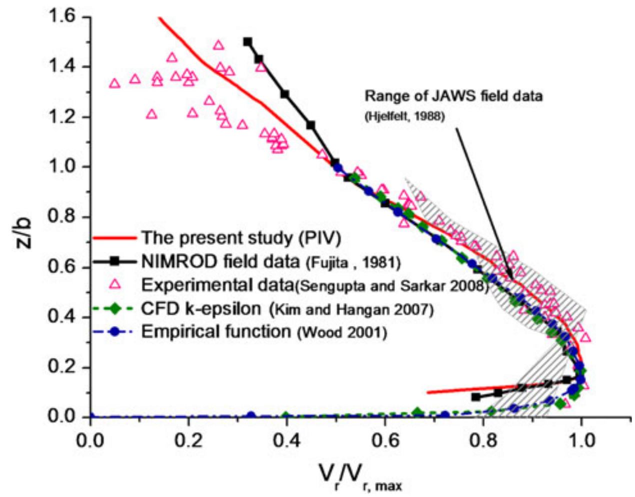

Fig. 6 The measured outflow velocity profile versus the field measurement data of microbursts occurring in nature and the published results of previous studies. For the vertical axis of the figure, the height above the ground is scaled by the height, *b*, at which the velocity is half the maximum

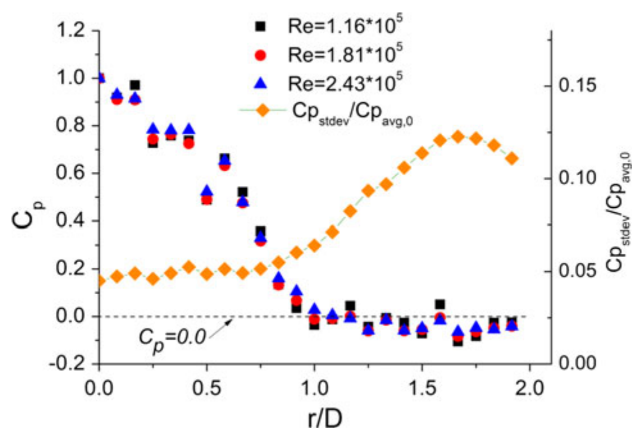

Fig. 7 The measured surface pressure distributions on the ground plane

the PIV measurement results given in Fig. 5, after impinging onto the ground plane, the high-speed diverging airflow was found to concentrate within a thin layer very close to the surface of the ground plane (i.e., Z/D < 0.25). Unlike conventional ABL winds with the wind speed increasing monotonically above the ground, the microburst-like wind was found to reach its maximum wind speed at a height very close to the ground surface (i.e., Z/D ≈ 0.06 for the present study) and then begin to decrease gradually as the height above the ground plate increases. Such extreme high-wind shear near the ground surface in microburst winds has been suggested to be the main reason to cause significant damages to low-rise civil structures on the ground.

From the measured normalized turbulent kinetic energy distribution shown in Fig. 5d, it can be seen clearly that the turbulence level within the core region of the microburst-like wind (i.e., r/D ≤ 0.5) is quite low. The turbulence intensity was found to increase greatly in the outflow region of the microburst-like wind (i.e., r/D > 1.0). A region with very high turbulence intensity (i.e., much higher turbulent kinetic energy) was found to exist at the downstream location of r/D ≈ 1.5–2.0. The high turbulence intensity in the region was found to be responsible for the significant surface pressure fluctuations and extreme wind load peaks acting on the building models when mounted in the region, which will be discussed later in the present study.

Figure 6 shows the quantitative comparisons of the measured outflow velocity profile of the microburst-like wind of the present study versus the NIMROD field measurement data of real microbursts occurring in nature along with the published data of previous studies. The outflow velocity profiles given in Fig. 6 were taken in the vicinity of the radial location where the maximum wind speeds in the microburst-like winds occur. As shown in Fig. 6, while the radial velocity of the microburst-like wind was normalized by the maximum radial velocity $V_{r,\ \max}$ (i.e., $V_r/V_{r,\ \max}$), the height where half of the maximum radial velocity occurred (i.e., $b \approx 170$ mm for the present study) was used to normalize the vertical height in the microburst-like wind (i.e., z/b). As suggested in previous studies, while the detailed flow features of each microburst may vary from case to case, all the microbursts were found to have a similar trend in terms of normalized outflow velocity profiles. It can also be seen clearly that even though the simulated microburst-like wind by using ISU microburst simulator and the real microbursts occurring in nature are significantly different in their size (e.g., the one generated by using ISU microburst simulator with a diameter of 0.6 m vs. approximately 400–4,000 m for the real microbursts in nature), the unique features of the outburst flows in microburst-like winds are captured reasonably well by using the impinging-jet-based ISU microburst simulator.

In the present study, the surface pressure distribution on the test ground plane induced by the microburst-like wind was also measured before the gable-roof building models were mounted on the ground plane. Figure 7 shows the measured surface pressure coefficients on the ground plate at three different Reynolds numbers (i.e., $Re = 1.2 \times 10^5$; $Re = 1.8 \times 10^5$, and 2.4×10^5 respectively). It can be seen that a high static pressure region (i.e., the region with higher positive C_p values), caused by the direct impinging of the core jet flow exhausted from ISU microburst simulator, exists on the ground plane near the core center of the microburst-like wind. The size of the high-pressure region was found to be much greater than the diameter of the impinging core jet flow (i.e., r/D < 0.5), which almost reached to the radial location of r/D ≈ 1.0. The surface pressures on the ground in the outburst flow further away from the core region of the microburst-like wind (i.e., r/D $\geq$ 1.0) were found to be quite small with the pressure coefficients (i.e., C_p values) being negative (i.e., the local surface pressure is slightly smaller than the atmospheric pressure). The measured surface pressure distribution on the ground plane was found to agree with that reported in Sengupta and Sarkar (2008) well. Similar surface pressure distributions were also reported in the previous studies of Tu and Wood (1996) and Baydar (1999).

Based on the comparison of the measurement results at three Reynolds numbers, it can be seen that the pressure distribution pattern on the ground plane was almost independent of the Reynolds number in the range used in the present study. The significant variations of the surface pressure on the ground plane induced by the microburst-like wind also indicate that the position of the building models (i.e., where the building models were mounted) with respect to the core center of the microburst-like wind will be an important factor to determine the surface pressure distributions and the resultant wind loads acting on the building models in the microburst-like wind.

In order to reveal the turbulent nature of the microburst-like wind more clearly, the fluctuation amplitudes of the surface pressure on the ground plate were also plotted in Fig. 7, where $C_{p,\mathrm{stdev}}$ is the standard deviation of measured pressure coefficients and $C_{p,\mathrm{avg},\ 0}$ is the averaged pressure coefficient at the impinging center (i.e., r/D $\approx$ 0). It can be seen clearly that while the fluctuation amplitude of the surface pressure on the ground plate was found to be relatively small in the core region of the microburst-like wind, the fluctuation amplitude was found to increase rapidly in the outburst region of the microburst-like wind and reach its maximum value at the downstream location of r/D $\approx$ 1.5–2.0. Such distribution trend of the surface pressure fluctuation on the ground plate is believed to be closely related to the high turbulence intensity levels of the microburst-like wind in the outburst flow as revealed clearly in the PIV measurement results given in Fig. 5. The significant fluctuation of the surface pressure on the ground plate in the outburst region would also imply that the surface pressure distributions on the building models would also fluctuate greatly when the test models were mounted in the outburst region of the microburst-like wind, which will be discussed later in the present study.

3.2 The effects of the locations of the building models with respect to the core center of the microburst-like wind

In the present study, the effects of the mounted locations of the gable-roof building models with respect to the core center of the microburst-like wind on the vortex structures and surface pressure distributions around the building models were also assessed quantitatively. While Fig. 8 gives the PIV measurement results to reveal the flow structures around the building models as they were mounted at different radial locations away from the center of the microburst-like wind, Fig. 9 shows the measured surface pressure coefficients around the building models at locations corresponding to the PIV measurements. For the measurement results given in the figures, the orientation angle of the models was set to be 0°, i.e., the oncoming microburst-like wind (radial outflow) would be perpendicular to the roof ridges of the building models along their centerlines as shown in Fig. 4.

It can be seen clearly that the flow characteristics and the surface pressure distributions around the gable-roof building models (thereby, resultant wind loads) would depend greatly on the locations of the building models with respect to the center of the microburst-like winds. As revealed clearly from the PIV measurement results given in Fig. 8a, when the models were mounted near the core center of the microburst-like wind (i.e., r/D $\approx$ 0), the vertically downward jet flow was found to be impinging directly onto the roofs of the models. As a result, the models were found to be completely wrapped by high positive pressures caused by the direct impingement of the jet flow, as shown clearly in Fig. 9a. The measured surface pressure distributions and flow features were found to be very similar for the two building models in spite of the different roof angles of the models. Corresponding to the high surface pressures on the roofs of the building models, the resultant aerodynamic forces would push the roofs downward to potentially cause roof collapse when the building models were mounted inside the core region of the microburst-like wind. It should be noted that the geometric center of ISU downburst simulator was identified before the PIV measurements were conducted, and the building models were tried to be mounted at the geometric center of ISU downburst simulator for the test cases of r/D $\approx$ 0. However, as shown in Fig. 8a, the PIV measurement results reveal that the building models were actually mounted at a location about 2 % off the center of the oncoming impinging jet flow for the test cases of r/D $\approx$ 0. This is a systematic error, which was be caused by the measurement error in identifying the geometric center of ISU downburst simulator or/and the non-uniformity of the oncoming impinging jet flow driven by the fan at the top of microburst simulator. It should be noted that this small systematic error will not affect the general discussions and findings derived from the present study.

As the building models were moved outward to the leading edge of the outburst flow of the microburst-like wind (i.e., r/D $\approx$ 0.5), the flow features around the building models were found to become quite different, as

Fig. 8 PIV measurement results with the building models mounted at different locations (*left*: building model with 16° roof angle; *right*: building model with 35° roof angle) **a** r/D ≈ 0.0 **b** r/D ≈ 0.5 **c** r/D ≈ 1.0 **d** r/D ≈ 1.50 **e** r/D ≈ 2.0

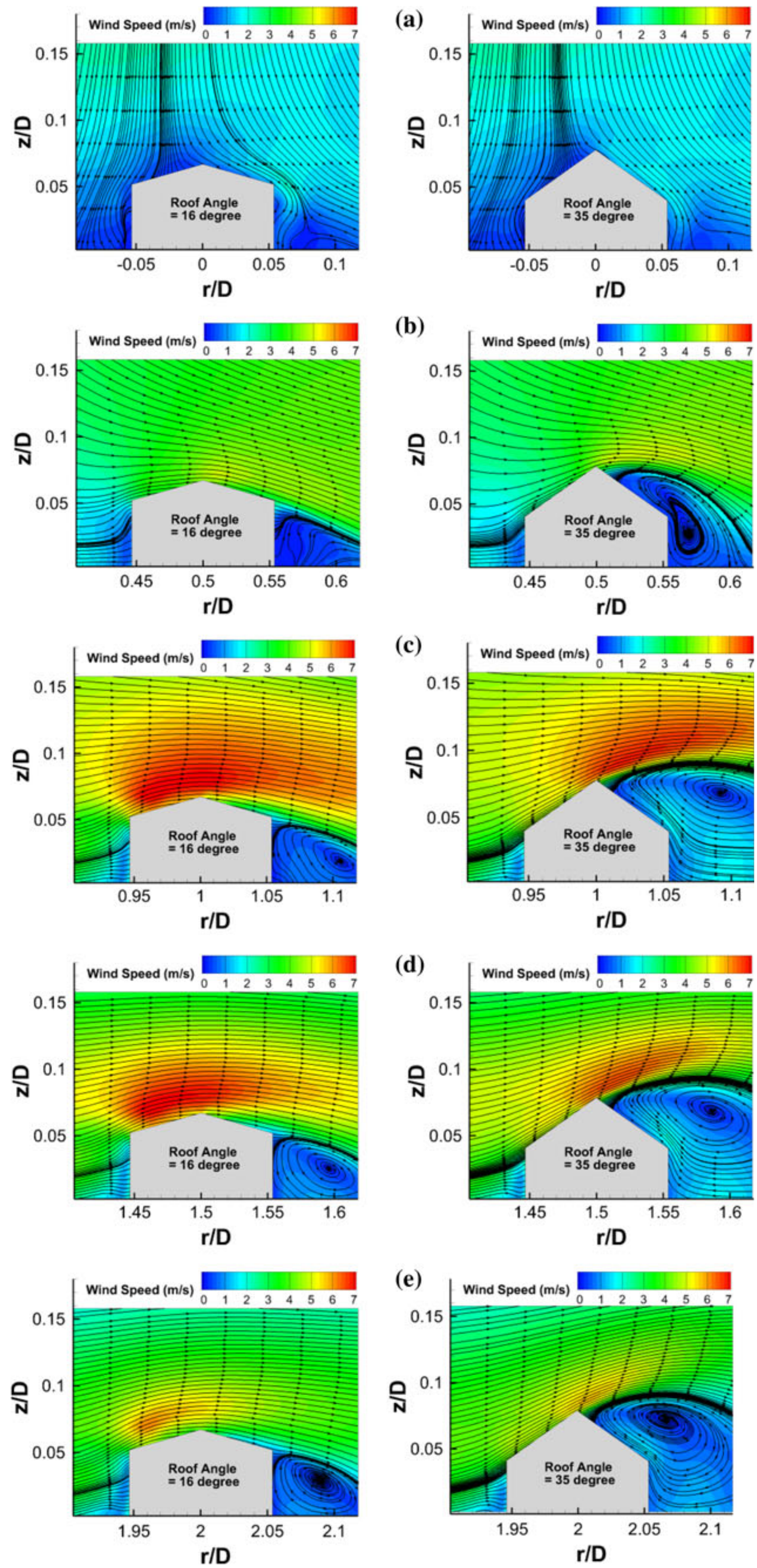

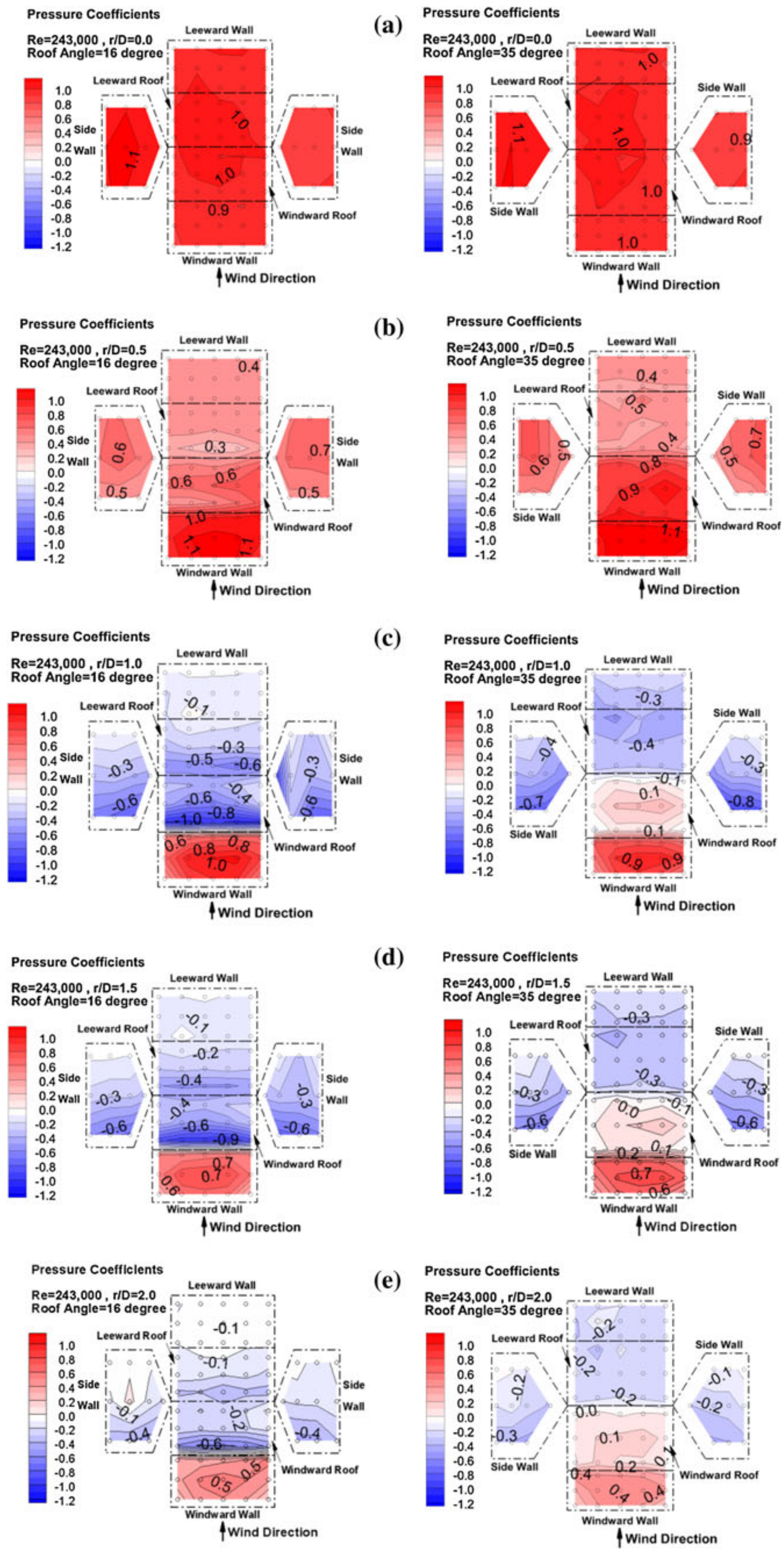

Fig. 9 Surface pressure distributions with the building models mounted at different locations (*left*: building model with 16° roof angle; *right*: building model with 35° roof angle) **a** r/D ≈ 0.0 **b** r/D ≈ 0.5 **c** r/D ≈ 1.0 **d** r/D ≈ 1.50 **e** r/D ≈ 2.0

revealed clearly from the PIV results given in Fig. 8b. While the flow streamlines far away from the building models were still found to be tilted downward, the streamlines near the ground plane were found to become horizontal and parallel to the ground plane. For the building model with 16° roof angle, the flow was found to stay attached to both the windward and leeward roofs of the building model. A small recirculation region was found in the wake of the model. For the model with 35° roof angle, the flow was found to separate from the leeward roof of the building model, which results in a much larger recirculation region in the wake of the model. While the surface pressures on roofs of the models were found to become much smaller when the models were moved away from the core center of the microburst-like wind, the effects of the roof angle can be seen easily from the surface pressure measurement results given in Fig. 9b. The surface pressures on both the windward and leeward roofs of the 35° roof model were found to be greater compared with those of the 16° roof model, which would result in a larger aerodynamic force to cause roof collapse for the 35° roof the model. It should also be noted that the surface pressure coefficients around the models were still found to be positive when models were mounted at the leading edge of the outburst flow of the microburst-like wind (i.e., r/D $\approx$ 0.5). Since the surface pressure coefficients on the back walls of the models (i.e., $C_p \approx 0.4$) were found to become much smaller compared to those on the front walls (i.e., $C_p \approx 1.0$) due to the existence of the recirculation zone in the wakes of the models, it is expected that the resultant aerodynamic force would push the models away from the center of the simulated microburst.

As seen in the PIV measurement results given in Fig. 8c, when the models were mounted in the outburst region at the location of r/D $\approx$ 1.0, while the oncoming flow was seemingly attached on both the windward and leeward roofs of the 16° roof model and the windward roof of the 35° roof model, the flow was found to separate from the roof ridge for the 35° roof model, which results in a very large recirculation zone in the wake of the model. The recirculation zone over the leeward roof of the model with 35° roof angle was found to become much greater than that of r/D $\approx$ 0.5 case, which resulted in much lower pressures on the leeward roof and back wall of the model. As shown in Fig. 9c, for the model with 16° roof angle, while the surface pressure coefficients on the front wall were found to be positive due to the direct impinging of the oncoming flow onto the front wall, the surface pressure coefficients on both the windward and leeward roofs, two side walls and back wall were found to become negative as the model was mounted at r/D $\approx$ 1.0. It indicates that the roof of the model would lift upward, instead of being pushed downward, when the model was mounted in the outburst flow of the microburst-like wind. For the model with 35° roof angle, the surface pressure coefficients on both the front wall and the windward roof were found to be positive. Corresponding to the much larger recirculation zone in the wake of the model, the pressure coefficients on the leeward roof and back wall were found to be lower for the model with 35° roof angle, compared to those of the model with 16° roof angle.

As the building models were moved further away from the center of the microburst-like wind (i.e., at the locations of r/D $\approx$ 1.5 and 2.0), while the local wind speed was found to become smaller, the streamlines of the flow were found to become tilted upward slightly as shown in Fig. 8d, e. It indicates that the airflow would have vertical upward velocity components in the outflow region far away from the core center of the microburst-like wind. As shown clearly in Fig. 9d, e, while the flow patterns around the building models were found to be quite similar to those of the r/D $\approx$ 1.0 cases, the absolute values of the surface pressure coefficients (for both the positive and negative surface pressure coefficients) around the models were found to become much smaller, corresponding to the smaller local wind speed at the radial locations.

In order to reveal the characteristics of the surface pressure distributions on the building models induced by the microburst-like wind more clearly, the measured surface pressures on the test models were compared with those in conventional ABL winds. Figure 10 shows the measured surface pressure profiles along the mid-planes of the two gable-roof building models with the models mounted at 4 different downstream locations (i.e., r/D $\approx$ 0.50, 1.0, 1.5 and 2.0) in the microburst-like wind. Since ASCE7-05 standard for minimum design loads (ASCE 2005) is widely used for wind load estimation of gable-roof buildings in conventional ABL winds, the standard values of the surface pressures given by ASCE 7-05 for the same gable-roof building models are also given in the figures for comparison. For the standard values of the surface pressures given by ASCE 7-05 standard, the surface pressure coefficient is defined as $C_{ph} = (P - P_{\text{atm}})/(0.5\rho U_h^2)$, where U_h is the wind speed at mean-roof-height of the building models.

As shown in Fig. 10, compared with those in conventional ABL winds as given by the ASCE 7-05 standard values, the surface pressures on the gable-roof building models would become much greater (almost twice) when the models were mounted near the leading edge of the outburst flow of the microburst-like wind (i.e., r/D $\approx$ 0.5). It indicates that with the same gable-roof building and the same wind speed at the mean-roof-height, the gable-roof buildings are much more likely to be damaged in microburst-like winds compared with the case in conventional

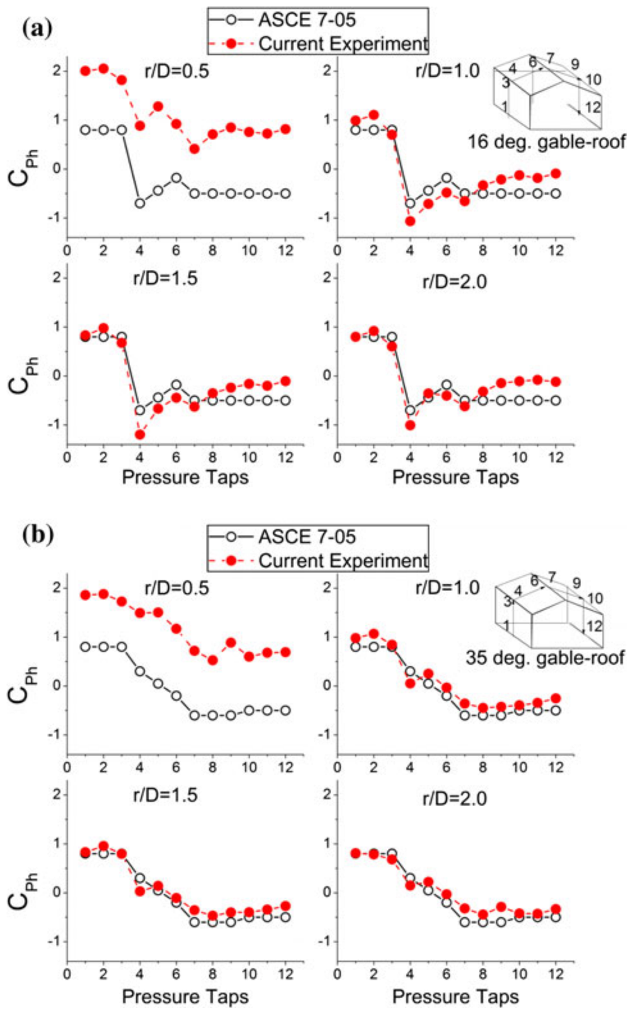

Fig. 10 The measured surface pressure coefficient profiles along the *centerlines* of the building models in microburst-like wind versus the standard values of ASCE 7-05 **a** the building model with 16° roof angle **b** the building model with 35° roof angle

ABL winds, due to the much higher surface pressure values (thereby, resultant wind loads) induced by the microburst winds.

As mentioned earlier, since the radial flow component would become dominant in the outburst flow with the corresponding streamlines becoming parallel straight-lines in the outflow region of the microburst-like wind, the characteristics of the outburst flow would become increasingly similar to a straight-line wind. As a result, when the gable-roof building models were mounted in the outflow region far away from the center of the microburst-like winds (i.e., r/D $\approx$ 1.0, 1.5, and 2.0), the measured surface pressure profiles on both the models were found to match with the ASCE 7-05 standard values reasonably well.

It should also be noted that unlike conventional ABL winds with the wind speed increasing monotonically above the ground, a microburst would produce an impinging-jet-like outflow profile with the maximum wind speed occurring at a much lower height close to the ground. As a result, when the 16° roof building model was mounted in the outflow region of the microburst-like wind, the measured surface pressures on the windward roof were found to be consistently lower, while the surface pressures on the leeward roof and back wall were found to be slightly higher, compared with the ASCE 7-05 standard values. The differences between the measured surface pressures and the ASCE 7-05 standard values were found to be much smaller for the building model with 35° roof angle.

3.3 The effects of the orientation angles of the building models with respect to the oncoming microburst-like wind

An experimental study was also conducted to assess the effects of the orientation angles (OA) of the gable-roof building models with respect to the oncoming microburst-like wind on the flow characteristics and the surface pressure distributions around the building models in the microburst-like wind. Figure 11 shows the measured surface pressure distributions on the two building models for OA of approximately 0.0°, 45.0°, and 90.0°, respectively. For the measurement results given in the figure, the building models were mounted in the outflow region of the microburst-like wind at r/D $\approx$ 1.0. As mentioned earlier, when the model with 16° roof angle was mounted in the microburst-like wind at OA $\approx$ 0.0°, the surface pressure coefficients on all the surfaces of the model except the front wall were found to be negative (i.e., the local surface pressures are lower than the atmospheric pressure). The surface pressures coefficients on the windward roof of the model with 35° roof angle were found to be positive in addition to the front wall, due to the direct impinging of the oncoming flow onto the roof with steeper angle. Corresponding to the much larger recirculation zone over the leeward roof of the model as revealed from the PIV measurement given in Fig. 8, the surface pressure coefficients on the leeward roof and rear wall of the 35° roof model were found to be much larger in magnitude compared with those of the building model with 16° roof angle.

When the building model with 16° roof angle was mounted at OA $\approx$ 45° with respect to the oncoming microburst-like wind, the surface pressure distribution on the windward roof of the building model was found to have a conical shape, which is similar to that of a building with a flat roof in a conventional ABL wind at an oblique angle, as described in Banks and Meroney (2001). According to Banks and Meroney (2001), due to the suction of the strong conical roof vortices, the roof corners are the most vulnerable to damage when the oncoming flow is at an oblique

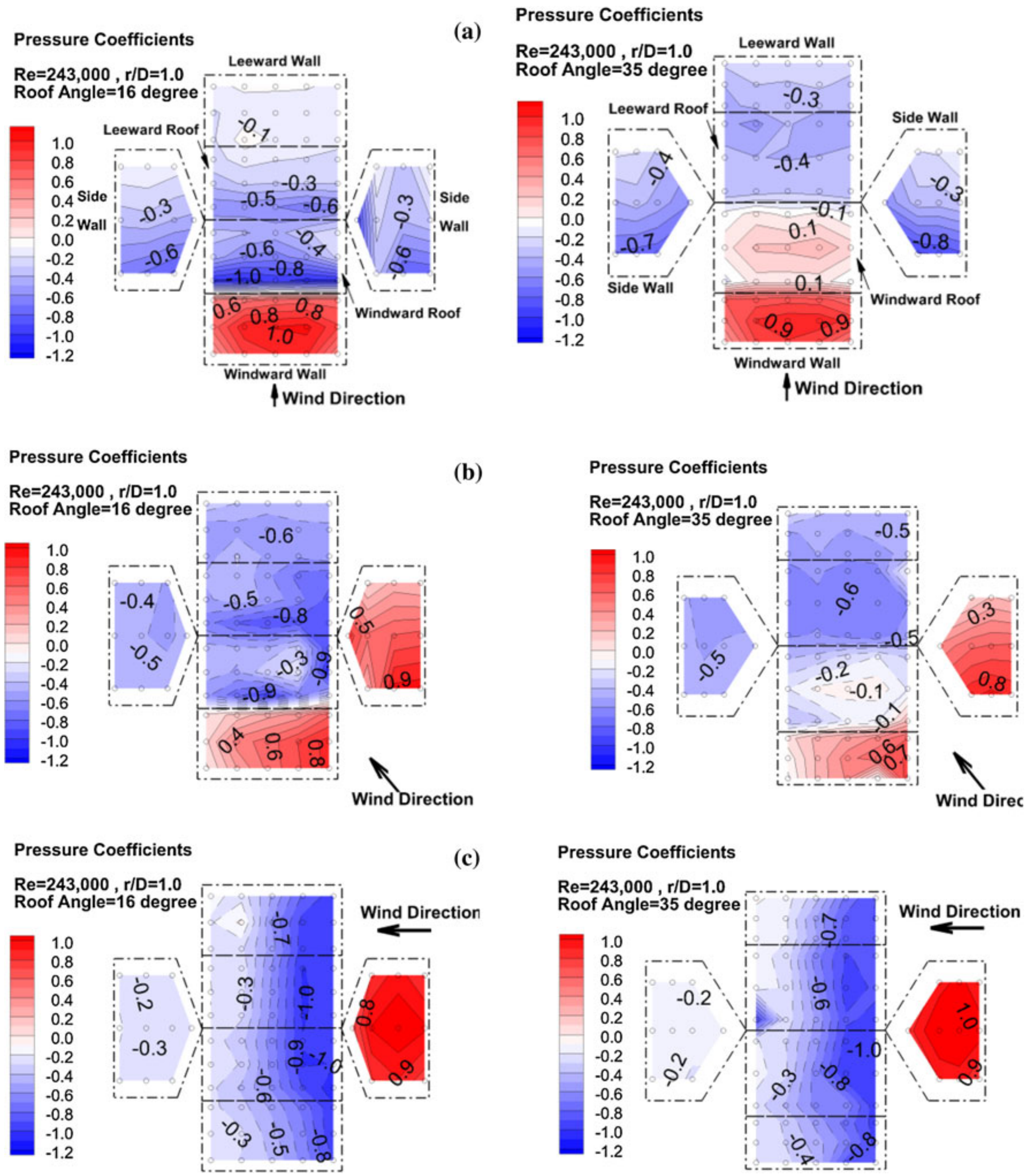

Fig. 11 The pressure distributions around the building models at different orientation angles. (*Left*: building model with 16° roof angle; *right*: building model with 35° roof angle) **a** OA ≈ 0° **b** OA ≈ 45° **c** OA ≈ 90°

angle with respect to the building axis. However, for the model with 35° roof angle, such conical-shaped pressure distribution could not be observed from the measured surface pressure distribution. Compared with those of the case with OA ≈ 0° having positive surface pressure coefficients on the windward roof, the surface pressure coefficients on the windward roof of the 35° roof building model were found to become negative when the building model was mounted at OA ≈ 45° with respect to the oncoming microburst-like wind.

When the two models were mounted at OA ≈ 90° with respect to the microburst-like wind, the oncoming flow would strike directly onto the gable-ended wall of the models, which results in the high-pressure coefficient values (i.e., Cp ≈ 0.8–1.0) on the windward walls. After impinging onto the gable-ended wall, the flow would separate at the roof edges along the joint between the roof and the walls. As a result, well-defined low-pressure bands were found on the roofs of the building models. Since the roof ridges of the models were aligned with the oncoming flow at OA $\approx$ 90°, the surface pressure distributions on the roofs as well as the side and back walls of the two models were found to be very similar in spite of different roof angles of the two building models.

Figure 12 shows some typical examples of the PIV measurement results to illustrate the flow features around the 35° roof model at OA $\approx$ 0° and 45° with respect to the oncoming flow in the microburst-like wind. For the PIV measurement results, the laser illumination plane was set within a horizontal plane at the half eaves height of the building model. It can been seen that when the model was mounted at OA $\approx$ 0°, the oncoming flow would strike onto the front wall of the model directly and then separate at the sharp corners of the building model, as expected. A recirculation zone was found to form in the wake of the model. The flow features and vortex structures around the gable-roof building model were found to be very similar to those reported by Hu et al. (2011) with a gable-roof building model placed in a conventional ABL wind. For the case with the building model mounted in the microburst-like wind at OA $\approx$ 45°, the oncoming flow was found to flow smoothly along the two side walls of the building model and then separate from the rear corners of the model, generating two very large recirculation bubbles in the wake. It should be noted that the two recirculation bubbles in the wake are similar to the sectional view of the two legs of a complicated 3D wake vortex formed in the wake of gable-roof buildings as revealed in Sousa and Pereira (2004). Since the flow features around the model for the case of OA $\approx$ 90° were found to be quite similar to those of the OA $\approx$ 0° case in the PIV measurement plane, the PIV measurement results for those cases are not presented here.

3.4 The characteristics of the resultant aerodynamic forces acting on the gable-roof building models in microburst-like wind

Based on the measured surface pressure distributions around the building models described above, the resultant wind loads (i.e., aerodynamic forces) acting on the models were determined by integrating the measured pressure distributions on the surfaces of the building models. Figures 13 and 14 give the radial and vertical components of the resultant aerodynamic forces acting on the building models as a function of the building location with respect to the center of the impinging jet. In the present study, the mean aerodynamic force coefficients, CF_r and CF_z, are defined as $CF_r = F_r/\left(0.5\rho U_{\text{jet}}^2 A_r\right)$ and $CF_Z = F_Z/(0.5\rho U_{\text{jet}}^2 A_Z)$, where F_r and F_Z are the mean values of radial and vertical components of the resultant aerodynamic forces acting on the models. A_r and A_Z are the projected areas of the models in r and Z directions as defined in Fig. 4. Since the azimuthal components of the resultant aerodynamic forces were found to be always insignificant due to the axis-symmetric nature of the oncoming microburst-like wind and the symmetry of the building models relative to the oncoming flows, thereby the measurement results are not presented here.

From the measurement results shown in Fig. 13, it can be seen that the variations of the radial components of the aerodynamic forces (i.e., F_r) acting on the models have a very similar trend for all the test cases. Since the streamlines of the airflow within the core region of the microburst-like wind were mainly vertically downward, the radial components of the resultant aerodynamic forces (i.e., F_r) were found to be very small when the models were mounted near the core center of the microburst-like wind. As revealed from the PIV measurements given in Fig. 5, the radial flow velocity component would increase rapidly as the distance from the core center of the microburst-like wind increases and become dominant in the outburst region (r/D > 0.5) of the microburst-like wind. The flow velocity was found to reach its maximum value at the location of r/D $\approx$ 1.0 and then decrease slowly with increasing radial distance from the core center of the microburst-like wind. As a result, the radial components of the aerodynamic forces acting on the building models (i.e., F_r) were found to increase rapidly, reach their peak values at the downstream

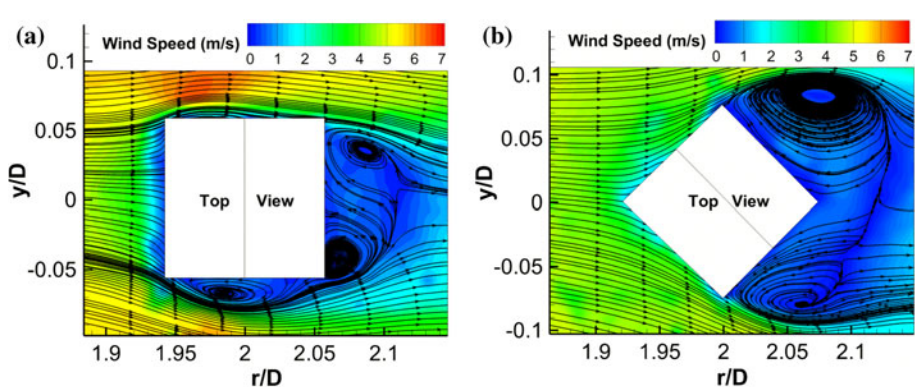

Fig. 12 Flow field around the 35° roof building model at different orientation angles with respect to the oncoming microburst-like wind. **a** OA $\approx$ 0° **b** OA $\approx$ 45°

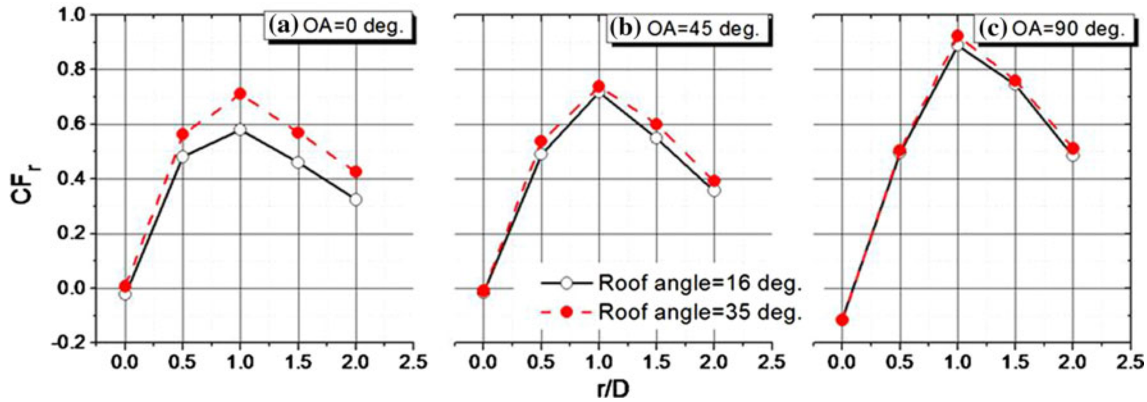

Fig. 13 Measured radial components of the aerodynamic forces acting on the building models

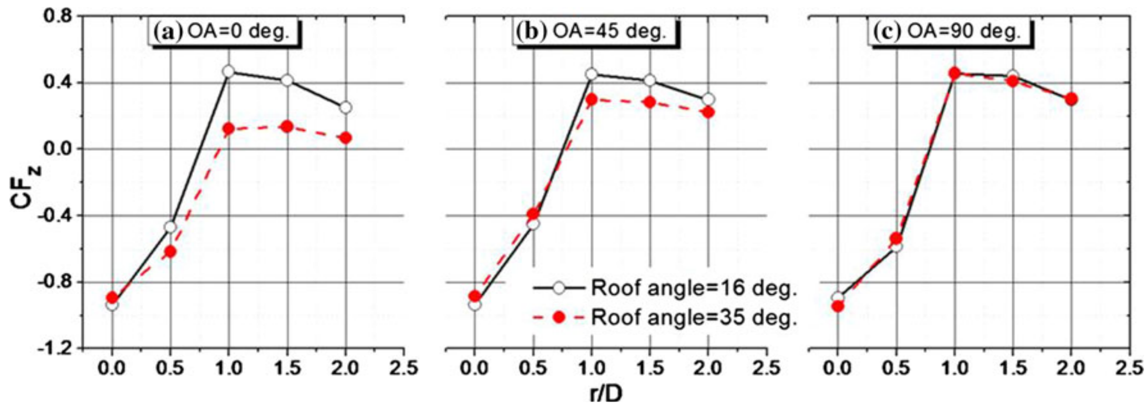

Fig. 14 Measured vertical components of the aerodynamic forces acting on the building models

location of r/D $\approx$ 1.0, and then decrease gradually due to the decreasing wind speed at the further downstream locations.

The effects of the roof angle on the resultant radial aerodynamic forces acting on the building models are also revealed clearly from the comparison of the measurement results given in Fig. 13. When the models were mounted at OA $\approx$ 0° with respect to the oncoming flow, the model with a larger roof angle (i.e., 35° roof building) was found to experience a greater radial aerodynamic force in the outwardly direction. As the orientation angle increases (i.e., for cases with OA $\approx$ 45° and 90°), the differences in the radial components of the resultant aerodynamic forces between the two building models with different roof angles were found to become smaller and smaller.

As shown from the measured surface pressure distributions given in Fig. 9a, the two gable-roof building models would experience high positive pressures over their envelopes (i.e., $C_P \approx 1.0$) when the models were mounted near the core center of the microburst-like wind (r/D $\approx$ 0.0), due to the direct impinging of the downdraft onto the models. Corresponding to the high surface pressures on the roofs, the vertical components (i.e., F_Z) of the resultant aerodynamic forces acting on the models were found to be quite significant, i.e., $CF_Z \approx -0.9$ to -1.0, as shown in Fig. 14. The negative sign of the CF_Z indicates that the resultant loads on the roof would be downward that would potentially cause collapse of the roof by pushing it down.

The variations of the vertical aerodynamic forces acting on the building models as a function of the position of the models are found to be closely related to the unique features of the microburst-like wind. As shown in Fig. 5, the surface pressures on the ground plane would decrease with the increasing radial distance away from the core center of the microburst-like wind. As a result, the magnitude of the resultant downward aerodynamic forces acting on the models was found to decrease rapidly as the building models were moved away from the core center the microburst-like wind. As shown in Fig. 14, when the models were moved into the outburst region of the microburst-like wind (i.e., at the radial position r/D $\geq$ 0.75), the coefficients of the vertical aerodynamic forces, CF_Z, were found to change their signs from negative to positive, which indicates that the resultant aerodynamic forces acting on the roof would be uplift. The uplift forces acting on the models were found to reach the peak values at the radial location of r/D $\approx$ 1.0 and then decrease slowly as the models were mounted further away from the core center of the microburst-like wind.

The effects of the roof angle and orientation angle of the building models on the vertical components of the resultant aerodynamic forces acting on the test models can also be seen clearly from the comparisons of the measurement results given in Fig. 14. It can been seen clearly that when the models were placed near the core center of the microburst-like wind (r/D ≈ 0.0), the vertical aerodynamic force coefficients of the two models, CF_Z, were found to be almost the same (i.e., $CF_Z \approx -1.0$) in spite of the different roof angles. As the building models were moved away from the core region into the outflow region of the microburst-like wind, the uplift forces acting on the model with smaller roof angle was found to be much greater than those with a larger roof angle when the models were mounted at OA ≈ 0° with respect to the oncoming microburst-like wind. The differences in the uplift forces were found to become smaller and smaller as the orientation angle increases.

In the present study, a set of experiments were also conducted to quantify the resultant wind loads acting on the building models at different Reynolds numbers of the microburst-like wind (i.e., $Re = 1.2 \times 10^5$–2.4×10^5) by changing the velocity of the impinging-jet flow exhausted from the microburst simulator. It was found that the characteristics of both radial and vertical aerodynamics forces acting on the models were be almost independent of the Reynolds number levels of the microburst-like wind within the range of the present study.

3.5 The fluctuations of the surface pressures on the gable-roof building models in microburst-like wind

While the time-averaged pressure measurement results given above are very helpful to reveal the global features of the wind loads acting on gable-roof buildings induced by violent microburst-like wind, it would be very insightful and essential to take the turbulent nature of the microburst-like wind into account in order to assess its damage potential more accurately. In the present study, the fluctuations of the surface pressures on the gable-roof models were also investigated for a better understanding of the turbulent of the microburst-like wind.

Figure 15a shows the time series of the instantaneous surface pressure measurement results obtained from the same pressure tap on the windward roof of the 16° roof model (i.e., the selected point #1 shown in Fig. 15b) as the building model was mounted at different radial locations in the microburst-like wind. It can be seen clearly that the instantaneous surface pressures at the same pressure tap would fluctuate much more significantly as the model was

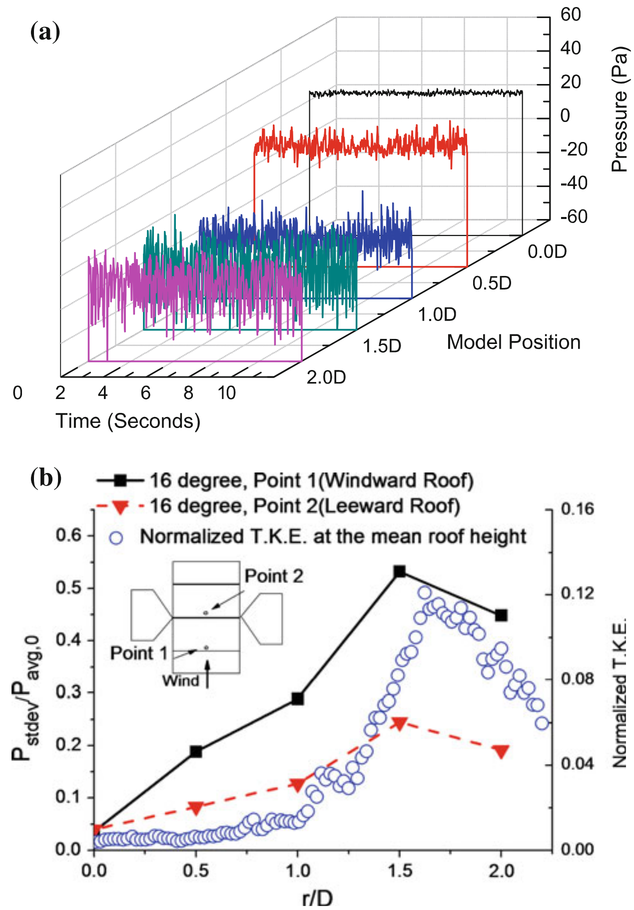

Fig. 15 Fluctuation of the surface pressures on the building model with 16° roof angle in the microburst-like wind **a** time series of the instantaneous surface pressure measurement results **b** the fluctuation amplitudes of the surface pressures at two selected points

moved away from the core region into the outburst region of the microburst-like wind.

The fluctuation amplitudes of the instantaneous surface pressures at two typical positions on the building model as a function of the radial location of the model with respect to the core center of the microburst-like wind are given in Fig. 15b. In this figure, P_{stdev} denotes the standard deviations of the instantaneous surface pressure data; $P_{avg,0}$ represents the time-averaged values of the surface pressure at the selected points when the model was mounted at the core center of the microburst-like wind (i.e., r/D ≈ 0). The turbulence kinetic energy level of the microburst-like wind at the mean roof height were also plotted in Fig. 15b in order to elucidate the close relationship between the characteristics of the surface pressure fluctuations on the building model and the variations of the turbulence level in the microburst-like wind. As revealed clearly in Fig. 15b, the fluctuation amplitudes of the surface pressures at the selected points were found to be quite small when the building model was mounted within the core region of the microburst-like wind, corresponding to the low turbulence level in the core region of the microburst-like wind. The amplitudes of the surface pressure fluctuations were found to increase very rapidly as the building model was moved away from the core region into the outburst region of the microburst-like wind and reach their maximum values at $r/D \approx 1.5$ due to the highest turbulence intensity at the downstream location. The pressure fluctuation amplitudes were then found to decrease as the model was moved further downstream, corresponding to the decreasing turbulence intensity level in the outflow region further away from the center of the microburst-like wind. From the comparison of the measurement results at the two selected points, it is interesting to note that the surface pressure fluctuations on the windward roof of the building model (i.e., Point #1) were found to be always greater than those on the leeward roof (i.e., Point #2). The observation was also believed to be closely related to the vortex structures and turbulent characteristics of the flow field around the building models in the microburst-like wind. Since Point #1 was located at the leading edge of the windward roof, the fluctuation of the surface pressure at this point was mainly determined by the turbulence intensity level of the oncoming microburst-like wind. However, since flow separation was found to occur over the ridge of the building model to form a large separation bubble sitting over the leeward roof as shown clearly in Fig. 8, the fluctuation of the surface pressure at Point #2 would be decoupled from the oncoming flow and affected mainly by the separation bubble on the leeward roof. A completely different outcome would be expected for the same building model when placed in a conventional ABL wind due to the significant difference in the flow characteristics of the oncoming flow (Hu et al. 2011). It should be noted that a larger fluctuation amplitude of the surface pressures on the same building model would imply a higher peak wind load acting on the building model, which would increase the damage potential of the gable-roof building in microburst-like wind. Since the characteristics of the surface pressure fluctuations on the building model with 35° roof angle were found to be very similar to those of the 16° roof angle model described above, the measurement results for the 35° roof model are not presented here.

It should be noted that while the present experimental study was conducted to investigate the near-ground flow characteristics of microburst-like winds and microburst-induced wind loads acting on low-rise buildings over a homogenous flat surface, the near-ground flow structures of the extreme wind events, such as tornadoes, hurricanes and microbursts, may also be affected strongly by the different terrains on the ground. The effects of the terrain conditions on the ground, such as the landscape features, surface roughness and thermal boundary conditions, on the near-ground flow structures of microburst-like winds and the microburst-induced wind loads acting on buildings will be investigated in the near future.

4 Conclusions

An experimental study was conducted to investigate the flow characteristics of microburst-like wind and to assess the resultant wind loads acting on low-rise gable-roof buildings induced by the microburst-like wind. The experiments were carried out by using an impinging-jet-based microburst simulator in the Department of Aerospace Engineering of Iowa State University with two gable-roof building models of different roof angles for the comparative study. In addition to measuring the surface pressure distributions (thereby, the resultant aerodynamic forces) around the building models, a high-resolution digital Particle Image Velocimetry (PIV) system was used to conduct flow field measurements to reveal the vortex structures and turbulent flow characteristics around the test models in the microburst-like wind. The effects of important parameters, such as the distance between the center of the microburst-like winds and the models, the roof angle and the orientation angles of the building models with respect to the oncoming microburst-like wind, and the Reynolds numbers of the microburst-like flow, on the characteristics of the flow fields and the surface pressure distributions around the building models as well as the resultant aerodynamic forces acting on the test models were assessed quantitatively.

The PIV measurements reveal clearly that the flow streams in the core region of the microburst-like wind, which are mainly vertical pointing downward before impinging onto the ground plane, would turn rapidly at right angle after impinging onto the ground plane. The flow streamlines were found to become parallel to the ground plane in the outflow region with high-speed flow concentrated within a layer close to the ground plate. While diverging from the core center of the microburst-like wind, the outburst flow was found to accelerate at first, reach its maximum wind speed at the location of $r/D \approx 1.0$, and then slow down gradually further downstream. While the turbulence intensity level inside the core region of the microburst-like wind was found to be quite small, the turbulence intensity was found to increase rapidly in the outburst flow region with highest turbulence intensity occurring at the location of $r/D \approx 1.5$. The high turbulence level in the outburst flow was found to be responsible for the significant fluctuations of the surface pressures on the building models when the models were mounted in the outflow region of the microburst-like wind.

It was also found that the surface pressure distributions and the resultant wind loads (i.e., aerodynamic forces) acting on the models would change significantly depending on the roof angles, the orientation angles, and the locations of the building models with respect to the core center of the microburst-like wind. When mounted within the core region of the microburst-like wind ($r/D \leq 0.5$), the building models were found to experience high positive pressures on the entire envelope due to the direct impinging of the vertically downward core jet flow onto the test models. The resultant aerodynamic force was found to be acting vertically downward on the roof. As the building models were moved away from the core region toward the outflow region of the microburst-like wind, while the vertical components of the resultant aerodynamic forces were found to decrease rapidly, the horizontal components of the aerodynamic forces were found to become bigger and bigger until reaching the peak values at $r/D \approx 1.0$. When the building models were moved further downstream (i.e., $r/D \geq 1.0$), while the magnitude of the aerodynamic forces acting on the models were found to decrease gradually corresponding to the decreasing wind speed, the vertical components of the resultant aerodynamic forces were found to become uplift forces. Compared with those in conventional atmospheric boundary layer (ABL) winds as specified in ASCE 7-05, the gable-roof building models were found to experience much higher (i.e., almost double) surface pressures, thereby much larger wind loads when the test models were mounted at the leading edge of the outburst flow of the microburst-like wind (i.e., $r/D \approx 0.50$). Since the flow characteristics of the microburst-like wind in the outflow region would become increasingly similar to conventional ABL winds, the measured surface pressure profiles on the building models were found to agree with the ASCE 7-05 standard values reasonably well when the test models were mounted in the outflow region far away from the core center of the microburst-like wind.

In addition to the time-averaged measurement results that revealed the global features of the microburst-like wind and the resultant wind loads acting on the building models induced by the microburst-like wind, the standard deviations of the measured instantaneous surface pressures on the building models were used to assess the turbulent nature of the microburst-like wind. It was found that corresponding to the high turbulence levels in the outburst flow of the microburst-like wind, the surface pressures on the models were found to fluctuate significantly as the models were mounted in the outflow region. The large fluctuation amplitudes of the surface pressures on the test models would imply significant peak wind loads acting on the building models, which would greatly increase the damage potential of low-rise gable-roof buildings subject to microburst-like wind.

Acknowledgments The project is funded by National Science Foundation (NSF) under award number CMMI-1000198. The authors also want to thank Mr. Bill Richard of Iowa State University for his help in manufacturing the test models and setting of the experiments.

References

Alahyari A, Longmire EK (1995) Dynamics of experimentally simulated microbursts. AIAA J 33(11):2128–2136

ASCE 7-05 (2005). ASCE standard, minimum design loads for buildings and other structures ASCE 7-05, American Society of Civil Engineers (ASCE), New York, USA

Atlas D, Ulbrich CW, Williams CR (2004) Physical origin of a wet microburst: observations and theory. J Atmos Sci 61:1186–1196

Banks D, Meroney RN (2001) A model of roof top surface pressure produced by conical vortices: model development. Wind Struct 4(3):227–246

Baydar E (1999) Confined impinging air jet at low Reynolds numbers. Exp Thermal Fluid Sci 19:27–33

Bluestein HB, Golden JH (1993) A review of tornado observations. The Tornado: its structure, dynamics, prediction and hazards, geophysics monogram, vol. 79, American Geophysics Union, p 19

Chay MT, Letchford CW (2002) Pressure distributions on a cube in a simulated thunderstorm downburst, part A: stationary downburst observations. J Wind Eng Ind Aerodyn 90:711–732

Chay MT, Albermani F, Wilson R (2005) Numerical and analytical simulation of downburst wind loads. Eng Struct 28:240–254

Choi ECC (2004) Field measurement and experimental study of wind speed profile during thunderstorms. J Wind Eng Ind Aerodyn 92:275–290

Das KK, Ghosh AK, Sinhamahapatra KP (2010) Investigation of the axisymmetric microburst flow field. J Wind Eng 7:1–15

Fujita TT (1979) Objectives, operations and results of project NIMROD. Preprint, 11th conference on severe local storms. Kansas City. Am. Meteor. Society

Fujita TT (1985) The downburst: microburst and macroburst. University of Chicago Press, Chicago

Hjelmfelt MR (1987) The microbursts of 22 June 1982 in JAWS. J Atmos Sci 44(12):1646–1665

Hjelmfelt MR (1988) Structure and life cycle of microburst outflows observed in Colorado. J Appl Meteorol 27(8):900–927

Holmes JD (June 1999) Modeling of extreme thunderstorm winds for wind loading of structures and risk assessment. Wind engineering into the 21st century, In: Larsen A et al. Proceedings of the 10th international conference on wind eng. eds. Denmark, pp 1409–1415

Holmes JD, Oliver SE (2000) An empirical model of a downburst. Eng Struct 22:1167–1172

Hu H, Yang Z, Sarkar P, Haan F (2011) Characterization of the wind loads and flow fields around a gable-roof building model in tornado-like winds. Exp Fluids 51(3):835–851

Kaimal JC, Finnigan JJ (1994) Atmospheric boundary layer flows: their structure and measurement. Oxford University Press, Inc., Oxford, pp 10–16

Kanda M, Maruta E (1993) Characteristics of fluctuating wind pressure on long low-rise buildings with gable roofs. J Wind Eng Ind Aerodyn 50:173–182

Kim J, Hangan H (2007) Numerical simulation of impinging jets with application to downbursts. J Wind Eng Ind Aerodyn 95:279–298

Letchford CW, Illidge G (June 1999) Turbulence and topographic effects in simulated thunderstorm downdrafts by wind tunnel jet. In: Larsen A, Larose GL, Livesey FM (eds) Wind engineering into the 21st century, proceedings of the tenth international conference on wind engineering. Denmark, pp 1907–1912

Letchford CW, Chay MT (2002) Pressure distributions on a cube in a simulated thunderstorm downburst, part B: moving downburst observations. J Wind Eng Ind Aerodyn 90:733–753

Liu Z, Prevatt DO, Aponte-Bermudez LD, Gurley K, Reinhold T, Akins RE (2009) Field measurement and wind tunnel simulation of hurricane wind loads on a single family dwelling. Eng Struct 31(10):2265–2274

Mason MS, Letchford CW, James DL (2005) Pulsed wall jet simulation of a stationary thunderstorm downburst, part a: physical structure and flow field characterization. J Wind Eng Ind Aerodyn 93:557–580

Nicholls M, Pielke R, Meroney R (1993) Large eddy simulation of microburst winds flowing around a building. J Wind Eng Ind Aerodyn 46:229–237

Peterka JA, Hosoya N, Dodge S, Cochran L, Cermak JE (1998) Area average peak pressures in a gable roof vortex region. J Wind Eng Ind Aerodyn 77–78(1):205–215

Savory E, Parke GAR, Zeinoddini M, Disney P (2001) Modelling of tornado and microburst-induced wind loading and failure of a lattic transmission tower. Eng Struct 23:365–375

Selvam RP, Holmes JD (1992) Numerical simulation of thunderstorm downdrafts. J Wind Eng Ind Aerodyn 44:2817–2825

Sengupta A, Sarkar P (2008) Experimental measurement and numerical simulation of an impinging jet with application to thunderstorm microburst winds. J Wind Eng Ind Aerodyn 96:345–365

Sousa JMM (2002) Turbulent flow around a surface-mounted obstacle using 2D–3C DPIV. Exp Fluids 33:854–862

Sousa JMM, Pereira JCF (2004) DPIV study of the effect of a gable roof on the flow structure around a surface-mounted cubic obstacle. Exp Fluids 37:409–418

Stathopoulos T, Wank K, Wu H (2001) Wind pressure provisions for gable roofs of intermediate roof slope. Wind Struct 4:119–130

Tu CV, Wood DH (1996) Wall pressure and shear stress measurements beneath an impinging jet. Exp Thermal Fluid Sci 13: 264–373

Uematsu Y, Isyumov N (1999) Wind pressures acting on low-rise buildings. J Wind Eng Ind Aerodyn 82:1–25

Vasiloff S, Howard K (2008) Investigation of a severe downburst storm near arizona, as seen by a mobile doppler radar and the KIWA WSR-88D. Weather Forecast 24:856–867

Wilson JW, Roberts RD, Kenssiger C, McCarthy J (1984) Microburst wind structure and evaluation of Doppler radar for airport wind shear detection. J Clim Appl Meteorol 23:898–915

Wood GS, Kwok CS, Motteram NA, Fletcher DF (2001) Physical and numerical modelling of thunderstorm downbursts. J Wind Eng Ind Aerodyn 89:535–552

Yang Z, Sarkar P, Hu H (2011) An experimental study of flow field around a high-rise building model in tornado-like winds. J Fluids Struct 27(4):471–486

Zhang Y, Sarkar PP, Hu H (2012) Experimental and numerical investigations on the flow characteristics of microburst-like winds. 50th AIAA aerospace sciences meeting including the new horizons forum and aerospace exposition 09–12 January 2012, Nashville, Tennessee, AIAA 20121197